Paleoceanography and Paleoclimatology

RESEARCH ARTICLE
10.1029/2023PA004618

A Comparison Study of Mg/Ca-, Alkenone-, and TEX_{86}-Derived Temperatures for the Brazilian Margin

A. Bahr[1], A. Jaeschke[2], A. Hou[1,3], K. Meier[1], C. M. Chiessi[4], A. L. Spadano Albuquerque[5], J. Rethemeyer[2], and O. Friedrich[1]

[1]Institute of Earth Sciences, Heidelberg University, Heidelberg, Germany, [2]Institute of Geology and Mineralogy, University of Cologne, Cologne, Germany, [3]Institute of Oceanography, National Taiwan University, Taipei, Taiwan (ROC), [4]School of Arts, Sciences and Humanities, University of São Paulo, São Paulo, Brazil, [5]Departamento de Geoquímica, Universidade Federal Fluminense, Niterói, Brazil

Abstract The reconstruction of accurate sea-surface temperatures (SST) is of utmost importance due to the ocean's central role in the global climate system. Yet, a number of environmental processes might bias reliable SST estimations. Here, we investigate the fidelity of SST reconstructions for the western tropical South Atlantic (WTSA) for the interval covered by Marine Isotope Stages (MIS) 6–5, utilizing a core collected off eastern Brazil at ~20°S. This interval was selected as previous SST estimates based on Mg/Ca ratios of planktic foraminifera suggested a peculiar pooling of warm surface waters in the WTSA during MIS 6 despite glacial boundary conditions. To ground-truth the Mg/Ca-based SST data we generated SST reconstructions on the same core material using the alkenone and TEX_{86} paleothermometers. Comparison with alkenone-based temperature estimates corroborate the previous Mg/Ca-based SST reconstructions, supporting the suggestion of a warm-water anomaly during MIS 6. In contrast, TEX_{86}-derived temperatures, albeit representing annual mean SST in recent core top samples, are up to 6°C colder than Mg/Ca- and alkenone-based SST reconstructions. We interpret the periods of anomalously cold TEX_{86}-temperatures as a result of a vertical migration of the TEX_{86} producers (heterotrophic marine Thaumarchaeota) toward greater water depths, following food availability during phases of enhanced fluvial suspension input. Likewise, the data suggest that alkenone-based SST are, albeit to a minor degree when compared to TEX_{86}, affected by river run-off and/or a seasonal bias in the growth season of haptophyte algae.

Plain Language Summary In this study, we investigate the accuracy of sea-surface temperature (SST) reconstructions for the western tropical South Atlantic (WTSA) for the interval covered by Marine Isotope Stages (MIS) 6–5—the penultimate glacial-interglacial cycle (ca. 190,000 to 70,00 years before present). This time interval was selected because previous SST estimates based on Mg/Ca ratios of planktic foraminifera suggested a pooling of warm surface waters in the WTSA during late MIS 6 despite the cold glacial conditions. To verify the Mg/Ca-based SST data, we generated temperature reconstructions from a core located off Eastern Brazil using two common paleothermometers that based on lipid biomarkers: alkenone and TEX_{86}. The alkenone-based temperature estimates agree with previous Mg/Ca-based SST reconstructions, supporting the existence of a warm-water anomaly in the WTSA during MIS 6. On the other hand, TEX_{86}-derived temperatures were up to 6°C colder than Mg/Ca- and alkenone-based SST reconstructions. This discrepancy might be a result of a vertical migration of the TEX86 producers toward greater water depths where they feed on particles of organic matter. These migrations into deeper waters occurred during phases of increased river run-off fluvial suspension input which enhanced surface primary productivity and facilitated vertical particle flux through the water column.

Key Points:

- Parallel Mg/Ca (*Globigerinoides ruber*), alkenone and TEX_{86}-based temperature estimates in the western tropical South Atlantic (WTSA) across Marine Isotope Stages (MIS) 6–5
- Mg/Ca and alkenones represent annual mean sea surface temperatures, but most TEX_{86}-based temperatures deviate to colder values
- Anomalous sea surface warming in the WTSA during late MIS 6 appears as a robust signal

Supporting Information:

Supporting Information may be found in the online version of this article.

Correspondence to:

A. Bahr,
andre.bahr@geow.uni-heidelberg.de

Citation:

Bahr, A., Jaeschke, A., Hou, A., Meier, K., Chiessi, C. M., Albuquerque, A. L. S., et al. (2023). A comparison study of Mg/Ca-, alkenone-, and TEX_{86}-derived temperatures for the Brazilian Margin. *Paleoceanography and Paleoclimatology*, *38*, e2023PA004618. https://doi.org/10.1029/2023PA004618

Received 2 FEB 2023
Accepted 4 AUG 2023

1. Introduction

The robust quantitative assessment of past sea-surface temperatures (SST) is one of the most crucial objectives of paleoceanography, as it is pivotal for understanding past changes in heat transport and for testing the skill of numerical climate models simulating past (and modern) climates. However, several studies have revealed significant offsets between different well-established SST proxies (e.g., Bard, 2001; Bova et al., 2021; Crivellari et al., 2019; Leduc et al., 2010) stressing the importance of understanding the environmental factors that might potentially bias a proxy signal archived in the sedimentary record. Such environmental factors are manifold. They may be related to the ecology of the organism and hence influence their seasonality and habitat depth (e.g.,

Bova et al., 2021; Ceccopieri et al., 2018; Cléroux et al., 2009; Crivellari et al., 2019). Environmental stress could also have an impact on the metabolic processes and alter the physico-chemical conditions under which a proxy carrier is produced (e.g., a foraminiferal test or a coccolithophoride lipid; Blanz et al., 2005; Ferguson et al., 2008). In addition, ocean currents are able to transport proxy carriers over large distances, providing allochthonous paleoenvironmental signals (Ausín et al., 2022; Benthien & Müller, 2000; Kusch et al., 2010; Mollenhauer et al., 2008), while (early) diagenetic processes will act differently on different types of proxies (Huguet et al., 2009; Pena et al., 2005; Regenberg et al., 2007).

In our study we assess the question of how proxy signals are biased by varying environmental parameters, considering that the boundary conditions potentially influencing a specific proxy signal might change over time (e.g., upwelling, insolation, or river run-off). Here, we compare temperature estimates obtained via three well-established methods: (a) the trace elemental composition (Mg/Ca) of surface-dwelling planktic foraminifera (*Globigerinoides ruber* pink); (b) the unsaturation index of alkenones ($U^{K'}_{37}$); and (c) the distributional variations in marine thaumarchaeotal membrane lipids (TEX_{86}). These proxies are measured in a sediment core collected from the western tropical South Atlantic (WTSA) that covers Marine Isotope Stages (MIS) 6–5.

A particular motivation for this study derives from the fact that previous studies indicated unusually warm SST leading to the last two deglaciations (particularly during late MIS 6) implying an anomalous heat accumulation in the WTSA (Hou et al., 2020b; Santos et al., 2017). This pooling of warm surface waters is interpreted to have strongly impacted continental precipitation on South America by shifting the convection centers and enhancing coastal rainfall (Arndt et al., 2022; Hou et al., 2020a). However, since the available records were based on a single SST proxy, namely Mg/Ca analysis of *G. ruber* (p), the question remains if these warm temperatures might reflect a warm-season bias of the Mg/Ca-derived temperatures during this interval. Notably, proxy records indicate distinct changes in environmental conditions (such as riverine sediment input, upwelling intensity) (Hou et al., 2020a; Portilho-Ramos et al., 2015) over this period in the WTSA which might have influenced the SST records. Hence, we aim to test the validity of the generated SST records. Furthermore, the MIS 6–5 period is an ideal time interval for studying seasonality-related proxy biases because precession (and thus summer insolation) amplitudes were larger than during MIS 1 and 2 (Laskar et al., 2004), creating larger seasonality. The larger seasonality may induce seasonal biases in both the Mg/Ca and $U^{K'}_{37}$ proxies as both are susceptible to for example, summer or winter biases (Bova et al., 2021; Leduc et al., 2010).

In addition, the selected study site at the eastern Brazilian Margin (at ∼20°S) is characterized by conditions typical of a relatively oligotrophic tropical ocean (Antoine et al., 1996) with moderate sediment input from land (Govin et al., 2012), moderate upwelling (Schmid et al., 1995) and low bottom current speeds (Garzoli et al., 2015). Hence, it is representative of a wide range of tropical settings. Moreover, the investigated sediment core contains sufficient abundances of foraminifera and organic compounds for calculating temperature estimates via the different utilized paleothermometry methods.

In summary, our study shows that Mg/Ca and $U^{K'}_{37}$-derived temperatures represent SST ($SST_{Mg/Ca}$ and $SST_{Uk'37}$, respectively) and show good agreement for most of the record, while TEX_{86}-derived temperatures (T_{TEX86}) are proposed to shift between mixed layer and thermocline temperatures across the record. We further find that terrestrial input appeared to have a distinct imprint on TEX_{86} records; during MIS 6, there was a direct input of glycerol dialkyl glycerol tetraether lipids (GDGTs) to the core location via terrestrial runoff, while during MIS 5, more effective vertical particle flux probably led to changes in the depth habitat of GDGT producing archaea. Our results confirm the occurrence of anomalously high SST during late MIS 6.

2. Oceanography of the Western Tropical South Atlantic

Surface waters of the WTSA are composed of warm, saline and oligotrophic Tropical Water ($T > 20$°C, $S > 36.40$) (Castro et al., 2006; Stramma and England, 1999). Modern annual mean SST and sea-surface salinity at the study site (20°21.807′S, 38°37.387′W) are 26.0 ± 0.5°C (Locarnini et al., 2018) and 37.1 ± 0.1 (Zweng et al., 2019), respectively. At present, the seasonal SST amplitude is 2.7°C, with the coldest SST (24.4°C) occurring during austral winter (July to September) and warmest temperatures (27.1°C) during austral summer (January to March) (Locarnini et al., 2018). Upper ocean circulation is dominated by the southward flowing Brazil Current (BC), which originates at ca. 10°S where the South Equatorial Current (SEC) splits into a southward flowing current (BC) and a northward-flowing current (North Brazil Current) (Peterson and Stramma, 1991; Rodrigues

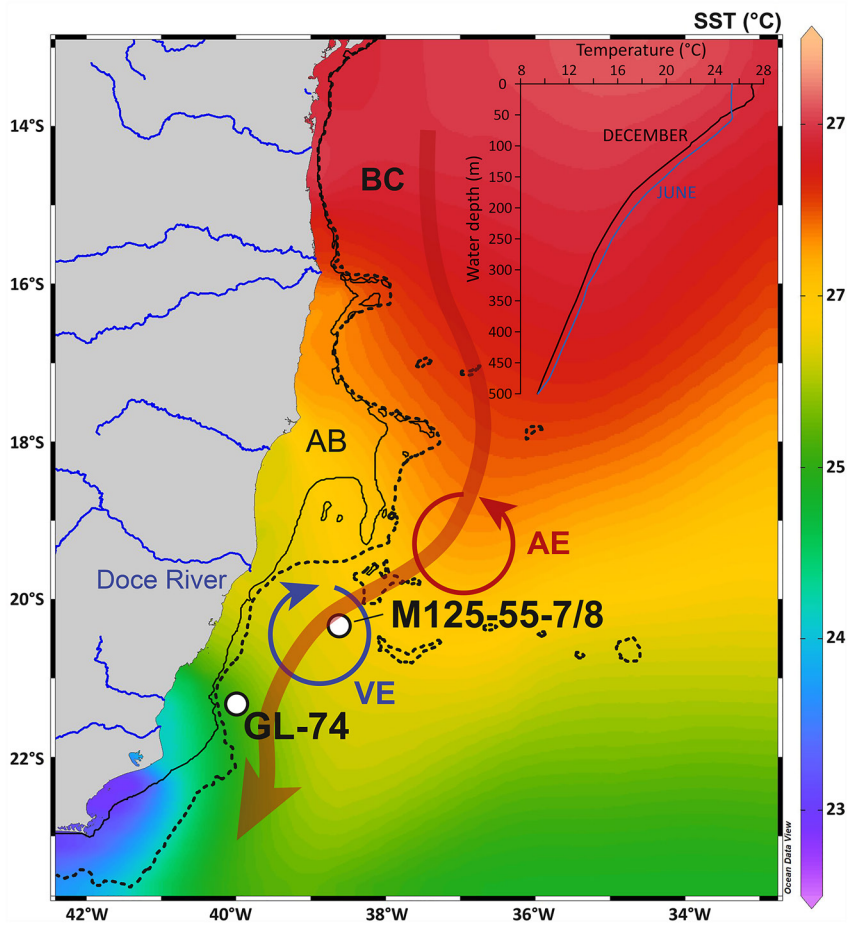

Figure 1. Sea-surface temperatures in the western tropical South Atlantic (Locarnini et al., 2018). Major surface hydrographic features are shown as arrows (Brazil Current, BC; the cold-core Vitória Eddy, VE, and warm-core Abrolhos Eddy, AE). Locations of piston core M125-55-7 and multicore M125-55-8 (this study) as well as core GL-74 (Portilho-Ramos et al., 2015) are indicated. The main river delivering terrigenous sediment to the investigated core site (i.e., Doce River) is labeled. Black stippled line: 150 m isobath indicating the shelf break; black thin line: 40 m isobath. AB, Abrolhos Bank. This figure was produced with Ocean Data View (Schlitzer, 2009). Insert: Vertical upper-ocean temperature profile at the study site for austral summer (red) and winter (blue), respectively (Locarnini et al., 2018).

et al., 2007; Stramma, 1989) (Figure 1). Volume transport within the BC varies seasonally, with maximum (minimum) transport during austral spring/summer (winter) when the ITCZ is displaced to the south (north) and the bifurcation of the SEC is shifted northward (southward) (Rodrigues et al., 2007).

Below ~200 m to a water depth of 500 m, the Tropical Water is underlain by the South Atlantic Central Water (SACW), which is characterized by a decrease in temperatures and salinities (20°C, 36.0 psu at 200 m to 5°C, 34.3 psu at 500 m; temperatures are shown in Figure 1) (Raddatz et al., 2020). The SACW is underlain by Antarctic Intermediate Water (AAIW; ~4°C, 34.3 PSU) while North Atlantic Deep Water, which has a higher salinity and oxygen concentration than AAIW (Mémery et al., 2000), is found below 1,100 m water depth. Below a water depth of ~4,000 m the Antarctic Bottom Water (AABW) constitutes the densest and deepest water mass in the WTSA (Stramma and England, 1999).

Important hydrological features of the study area are local upwelling cells generated by the interaction of the BC with the Abrolhos Bank and the Vitória-Trindade Ridge at 17°S–18°S. Both act as shallow topographic barriers and generate cyclonic meanders and eddies over the shelf as well as to the east and south of the Abrolhos Bank, that is, the warm-core Abrolhos Eddy and cold-core Vitória Eddy (Figure 1) (Arruda et al., 2013; Schmid et al., 1995). The study site locates within the Vitória Eddy which is most intense during austral spring/summer when the BC flow is strongest (Arruda and da Silveira, 2019). The cyclonic Vitória Eddy is characterized by

upwelling of cold (up to 8°C cooler in the eddy center), and low-salinity waters with high nutrient concentrations (Gaeta et al., 1999; Schmid et al., 1995).

Sediment input to the study area is dominated by siliciclastic material brought by the Doce River (Figure 1). The discharge of the Doce River is highly seasonal with maximum runoff occurring during the development of the South American summer monsoon in austral summer, and minimum runoff during austral winter (Oliveira and Quaresma, 2017).

3. Materials and Methods

3.1. Piston Core M125-55-7 and Parallel Multicore M125-55-8

The 1,175 cm long piston core M125-55-7 was retrieved in March 2016 during R/V METEOR cruise M125 at 20°21.807′S, 38°37.387′W from a water depth of 1,960.8 m (Bahr et al., 2016) (Figure 1). Core M125-55-7 consists of bioturbated clay to silty clay varying between dark and light gray in color without visible hiatuses. The piston core was used to produce the time series for MIS 6 and 5 presented here. The uppermost two cm of the parallel multicore M125-55-8 (from the same cruise and location) was used for assessing how our proxies recorded modern conditions at the study site.

3.2. Methods

3.2.1. Lipid Biomarker Analyses

Samples for lipid biomarker analysis were taken at approximately 2.5 cm resolution from the depth interval 559.5 to 202.5 cm core depth of piston core M125-55-7. Additionally, we collected two samples from multicore M125-55-8 at 0–1 and 1–2 cm to assess modern hydrographic data at the study site. Freeze-dried and ground sediment samples (ca. 7 g) were ultrasonically extracted using a 2:1 mixture of dichloromethane (DCM) and methanol (MeOH), repeated three times. The extracts were combined and the solvent was subsequently removed by rotary evaporation under vacuum. The resulting total lipid extracts were separated into apolar (with *n*-hexane), ketone (with DCM) and polar (with DCM:MeOH; 1:1) fractions using silica gel chromatography. After drying, the apolar and ketone fractions were dissolved in *n*-hexane prior to analysis. The polar fractions containing GDGTs were dissolved in *n*-hexane:isopropanol (95:5, v:v) and filtered through 0.45 µm polytetrafluorethylene (PTFE) syringe filters prior to analysis.

3.2.1.1. Alkenone and n-alkanes

Alkenone and *n*-alkane analyses were carried out on an Agilent 7890 series II gas chromatograph equipped with an on-column injector and a Flame Ionization Detector (GC-FID). A fused silica capillary column (DB-5MS; 50 m × 0.2 mm, film thickness: 0.33 µm) was used with He as carrier gas. The samples were injected at 70°C, and the consecutive GC oven temperature was raised to 150°C at a rate of 20°C/min. By 150°C the temperature increase was reduced to 6°C/min to 320°C, which was held for 40 min. Alkenones and *n*-alkanes were quantified using authentic external standards (2-nonadecanone, *n*-alkane (C_{21}–C_{40}) standard mixture; Supelco). Analytical precision based on replicate analyses of an in-house sediment standard was <0.2°C. Reproducibility of alkenone and *n*-alkane concentrations was generally <5% independent of total concentration.

The $U^{K'}_{37}$ index, which is based on the relative abundance of di- and tri-unsaturated alkenones produced by coccolithophorides in the surface ocean (e.g., Brassell et al., 1986) was calculated according to Prahl and Wakeham (1987):

$$U^{K'}_{37} = (C_{37:2})/(C_{37:2} + C_{37:3})$$

$U^{K'}_{37}$ values were converted in SST using the global core top calibration of Müller et al. (1998):

$$\mathrm{SST}\,(°\mathrm{C}) = \left(U^{K'}_{37} - 0.044\right)/0.033$$

The mean standard error of temperature estimation is ±1.5°C (Müller et al., 1998).

Regarding the $SST_{Uk'37}$ estimates we also tested the equation recently published by Novak et al. (2022) which uses a Bayesian approach:

$$U^{K'}_{37} = 0.032\,\mathrm{SST} + 0.081$$

The resultant $SST_{Uk'37}$ records based on the equations from Müller et al. (1998) and Novak et al. (2022) are very similar to each other (Figure S1 in Supporting Information S1), with an offset of approx. 0.4°C toward colder temperatures of the values produced with the equation by Novak et al. (2022) when compared to those produced with the equation by Müller et al. (1998). To allow comparison with published $SST_{Uk'37}$ we use the calibration method of Müller et al. (1998).

3.2.1.2. GDGTs

GDGTs were analyzed using ultra-high performance liquid chromatography (UHPLC; Agilent 1290 Infinity II) coupled to an Agilent 6460 Triple Quadrupole Atmospheric Pressure Chemical Ionization Mass Spectrometer (QQQ APCI MS) according to the method described by Hopmans et al. (2016). Improved separation of 5- and 6-methyl branched GDGTs (brGDGTs) was achieved by using two UHPLC silica columns coupled in series (BEH HILIC columns, 2.1 × 150 mm, 1.7 µm; Waters) connected with a pre-column of the same material maintained at 30°C at a flowrate of 0.2 ml/min. Individual GDGTs were detected via single ion monitoring (SIM; cf. Schouten et al., 2007) using *m/z* 744 for the internal standard, *m/z* 1,302, 1,300, 1,298, 1,296, and 1,292 for isoprenoid (iso)GDGTs including crenarchaeol and *m/z* 1,050, 1,048, 1,046, 1,036, 1,034, 1,032, 1,022, 1,020, and 1,018 for brGDGTs. Concentrations of GDGTs were calculated using an internal C_{46} standard (Huguet et al., 2006) and assuming a similar mass spectrometric response for all measured lipids. Reproducibility of GDGT concentrations was <9%.

GDGTs are membrane lipids synthesized by both aquatic archaea and terrestrial bacteria. The TEX_{86} index is based on the relative distribution of isoGDGTs produced by marine Thaumarchaeota in the upper water column and shows a relationship between molecule cyclization and SST (Schouten et al., 2002):

$$TEX_{86}^{H} = \log\left(\left([GDGT-2]+[GDGT-3]+\left[cren'\right]\right)/\left([GDGT-1]+[GDGT-2]+[GDGT-3]+\left[cren'\right]\right)\right)$$

Where GDGT-*n* denotes the number of rings (1–3) of the molecule and cren' refers to the crenarchaeol isomer (with 4 cyclopentane moieties and 1 cyclohexane group). The TEX_{86}^{H} was converted into SST using the high-temperature equation proposed by Kim et al. (2010) for high temperatures from 15 to 30°C as prevailing in the research area:

$$T_{TEX\_H} = 38.6 + 68.4\,TEX_{86}^{H}$$

The global core-top calibration has a mean standard error of ±2.5°C. As TEX_{86} may record subsurface temperatures, a depth-integrated (0–200 m) temperature calibration (T^{0-200}) from Kim et al. (2012) was also used:

$$T_{TEX\_0-200} = 30.7 + 54.7\left(TEX_{86}^{H}\right)$$

The mean standard error of estimate of the 0–200 m calibration is ±1.1°C. Analytical precision based on repeated measurements of an in-house sediment standard was <0.2°C.

We also applied the Bayesian SST calibration of the TEX_{86} proxy by Tierney and Tingley (2014), which resulted in a similar but on average 1.1°C colder temperature pattern compared to T_{TEX_H}, however, with an error of ca. ±5°C (cf. Figure S2 in Supporting Information S1). Given the similarity of both estimates and the smaller error of T_{TEX_H}, we will use the calibration of Kim et al. (2012).

The branched and isoprenoid tetraether (BIT) index was calculated as defined by Hopmans et al. (2004):

$$BIT = [I+II+III]/[I+II+III]+[Cren]$$

The roman numerals I, II, and III refer to brGDGTs originating from terrestrial soil bacteria, while Cren refers to the characteristic isoGDGT crenarchaeol of aquatic Thaumarchaeota. The BIT index is used to assess the relative input of terrestrial organic matter to marine environments and ranges from 0 (exclusively marine organic matter) and 1 (exclusively terrestrial organic matter) (Hopmans et al., 2004).

3.2.2. Faunal Analysis

Faunal counts of three selected and ecologically significant species were obtained between 545 and 220 cm core depth in 5 cm intervals of piston core M125-55-7. After freeze-drying, the samples were wet-sieved over a 63 µm mesh and oven-dried overnight at 40°C. Dried sediments of the size fraction 250–315 µm obtained via dry

sieving were split using an ASC microsplitter into aliquots with a total abundance of planktic foraminifera of at least 300 specimens. Counting of the complete split sample was subsequently done under a stereo microscope, distinguishing between *Globigerina bulloides*, which is affiliated with nutrient rich surface waters typically associated with upwelling conditions (Peeters et al., 2002; Salgueiro et al., 2008; Shrivastav et al., 2016), *Globigerinoides ruber* (pink) and *G. ruber* (white) which are affiliated with the oligotrophic and warm waters carried by the BC (Jentzen et al., 2019; Portilho-Ramos et al., 2015; Schmuker and Schiebel, 2002).

3.2.3. Stable Isotope Analysis

In order to improve the existing benthic foraminiferal stable oxygen isotope ($\delta^{18}O$) stratigraphy of MIS 6, the transition to MIS 5e (i.e., Termination II) and MIS 5e, 14 samples were selected between 490 and 420 cm core depth, alternating with previously analyzed samples (cf. Hou et al., 2020b) of piston core M125-55-7. In addition, we obtained stable carbon isotope measurements on both, the new as well as the samples published in Hou et al. (2020b). For stable isotope analyses, three benthic *Uvigerina* sp. specimens were picked from the >315 µm size fraction. Benthic foraminifera tests were gently crushed to expose shell chambers and rinsed three times with ultrapure ethanol and ultrasonicated between each wash. Stable carbon and oxygen isotopes were measured with a ThermoFisher Scientific MAT 253 Plus isotope ratio mass spectrometer coupled to a Kiel IV carbonate preparation line at the Institute of Earth Sciences, Heidelberg University (Germany). Measurements were calibrated to an in-house carbonate standard (Solnhofen limestone). Analytic precision based on repeated measurements of the in-house standard is 0.06‰ for $\delta^{18}O$ and 0.03‰ for $\delta^{13}C$.

3.2.4. Statistical and Time Series Analyses

Correlation coefficients between various proxy records were computed using the function "surrogateCor" implemented in the R-package "astrochron" (Meyers, 2014). Prior to analysis, the data series were resampled to a common time series based on the data set with fewer points. The estimated Pearson's correlation coefficient (r) is based on 10,000 iterations. The significance of the correlation (p) is calculated using the method of Ebisuzaki (1997).

4. Age Model

The age model used in this study is based on the benthic foraminiferal $\delta^{18}O$ stratigraphy published in Hou et al. (2020b). To enhance the robustness of the stratigraphy, the sample resolution during the target interval MIS 6–5 was enhanced to produce a better confined Termination II and MIS 5e, which are both intervals characterized by low sedimentation rates (Figure 2). Sedimentation rates for the interval MIS 6–5 average 2.9 cm/kyr, with a minimum during MIS 5e (0.5 cm/kyr) and a maximum of 5.6 cm/kyr during MIS 5c. While the new age model now provides better constraints on the duration of MIS 5e and the position of Termination II, it does notably not affect the conclusions of Hou et al. (2020a, 2020b), which are concerned with long-term (orbital-scale) processes.

5. Results

5.1. Temperature Estimates

The $SST_{Mg/Ca}$ from Core M125-55-7 and multicore M125-55-8 as published in Hou et al. (2020b) are based on the species-specific calibration provided by Dekens et al. (2002), which accounts for reductive and oxidative cleaning. Core top $SST_{Mg/Ca}$ estimates based on *G. ruber* (*p*) are 27.2 ± 0.92°C (based on replicate analyses; Hou et al., 2020b) (Table 1) and are within the error range of annual mean SST (26.0 ± 0.5°C) (Locarnini et al., 2018), although $SST_{Mg/Ca}$ may show a potential bias toward the austral summer. As described in Hou et al. (2020b), $SST_{Mg/Ca}$ are relatively stable over the period MIS 6–5 with no clear glacial/interglacial pattern (Figure 3). A remarkable feature is the broad plateau of high $SST_{Mg/Ca}$ of around 28.0°C during late MIS 6 until the end of MIS 5e. Notably, the $SST_{Mg/Ca}$ maximum is reached at ~137, 10 kyr before the climate optimum of MIS 5e. Minimum $SST_{Mg/Ca}$ values of ~25.5°C occurred during the global cold phases of early MIS 6, late MIS 5c and MIS 5a. Thus, the $SST_{Mg/Ca}$ clearly indicate that piston core M125-55-7 has been continuously under the influence of the warm BC.

Considering both, the long-term trend and absolute values, $SST_{Uk'37}$ closely follows $SST_{Mg/Ca}$ during MIS 6 and MIS 5e-d, including the early peak of $SST_{Uk'37}$ before the onset of MIS 5e (Figure 3). During this time interval, $SST_{Uk'37}$ are on average 0.4°C colder than $SST_{Mg/Ca}$, which fits to the core top $SST_{Uk'37}$ values of 26.6°C (Table 1), which are 0.3°C colder than core top $SST_{Mg/Ca}$ values and thus more closely aligned to annual mean

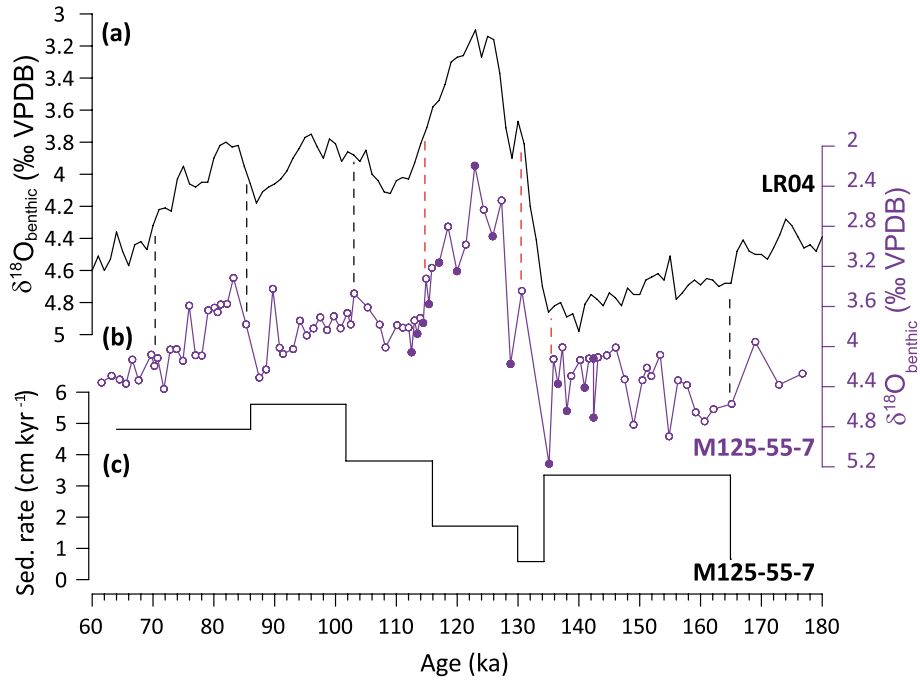

Figure 2. Age model of Core M125-55-7 (cf. Hou et al., 2020b) modified in the transition from Marine Isotope Stages 6 to 5, based on the stable oxygen isotopic analyses of additional samples of benthic foraminifera. (a) LR04 benthic isotope stack (Lisiecki and Raymo, 2005). (b) Benthic foraminifera stable oxygen isotope ($\delta^{18}O$) record from Core M125-55-7 obtained from *Uvigerina* sp. of Hou et al. (2020b) (open symbols), together with the new samples analyzed here (filled symbols). Tie points used in Hou et al. (2020b) are indicated by black dashed lines and the tie points revised in this study are shown by red dashed lines. (c) Sedimentation rates of core M125-55-7.

SST. However, distinct deviations between both proxy records occur between 150–140 ka and in particular during 109–89 ka and after 75 ka, when $SST_{Uk'37}$ are up to 4°C colder than contemporaneous $SST_{Mg/Ca}$.

The core top values of T_{TEX86_H} average to 26.5°C (Table 1) which is very close to $SST_{Uk'37}$ and would thus support the assumption that modern T_{TEX86} represent annual mean SST. The core top $T_{TEX86\_0\text{-}200}$ (22.0°C), on the other hand, is 2.4°C colder than the integrated temperature (24.4°C) of the upper 200 m at the study site (Locarnini et al., 2018) (Figure 1). Hence, our data is not in line with observations from the southern portion of the eastern Brazilian Margin at ca. 22°S where T_{TEX86} appears to be well correlated to both mixed-layer temperatures and thermocline-temperatures integrated between 100 and 200 m water depth (Ceccopieri et al., 2018). Instead, it supports findings by Crivellari et al. (2018) from the northern Brazilian Margin (6°N), where T_{TEX86} reflects mixed-layer temperatures (cf. also Hurley et al., 2018; Zhang and Liu, 2018). While the different paleotemperature proxies provide similar core top estimates at our study site, and all three agree with annual mean SST, the TEX_{86_H}-based temperature fluctuations deviate distinctly from SST trends reconstructed by both of the other methods (cf. gradient to $SST_{Uk'37}$, Figure 3), showing much higher variability and colder temperatures despite using the T_{TEX86_H} calibration. Particularly notable is a cooling in T_{TEX86_H} relative to $SST_{Mg/Ca}$ and $SST_{Uk'37}$ during early MIS 6 (195–157 ka) followed by a strong warming (by 6°C) during MIS 6 until Termination II at ~134 ka. The subsequent sharp T_{TEX86_H} decline to temperatures similar to early MIS 6 levels starts nearly 10 kyr before MIS 5e and reaches a minimum at the transition MIS 5e/d. Fluctuations of ~5°C (T_{TEX86_H}) occur during MIS 5d-a that, however, do not adhere to warm and cold MIS 5 substages but rather display a pacing that mirrors Ti/Ca fluctuations (Hou et al., 2020a) (Figure 4).

Table 1
Core Top Sea-Surface Temperatures (SST), Temperatures (T), and Branched and Isoprenoid Tetraether (BIT) Index From Multicore M125-55-8

Depth (cm)	$SST_{Uk'37}$ (°C)	$T_{TEX86\_0\text{–}200m}$ (°C)	T_{TEX86_H} (°C)	$SST_{Mg/Ca}$ (°C)	BIT
0–1	26.6	23.5	26.8	27.6	0.06
1–2	n.d.	20.5	26.2	26.8	0.07
Mean	26.6	22.0	26.5	27.2	0.07

Note. Modern annual mean SST for the study site is 26.0 ± 0.5°C, integrated temperature for 0–200 m water depth is 24.4°C (Locarnini et al., 2018).

5.2. Terrigenous Input

Core-top BIT values are low (0.07; Table 1). This is different from the MIS 6–5 interval where BIT values are mostly above 0.3 (Figure 4), which is considered

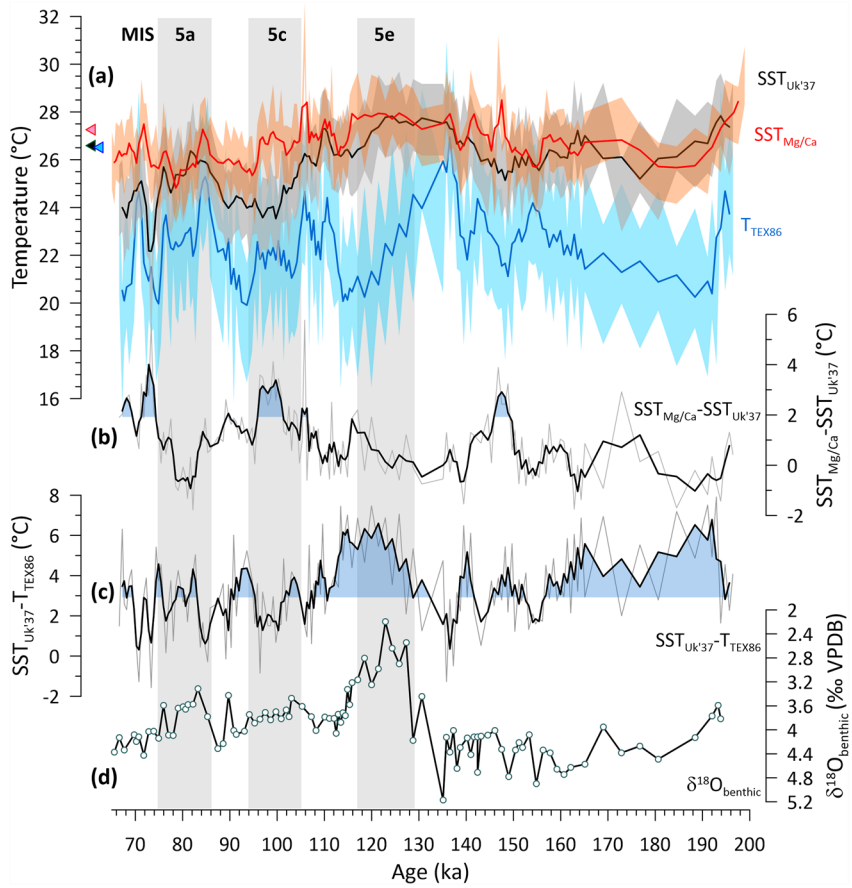

Figure 3. Temperature estimates and benthic foraminiferal stable oxygen isotopes ($\delta^{18}O$) from piston core M125-55-7 for Marine Isotope Stages (MIS) 6–5. (a) Mg/Ca-based sea-surface temperatures ($SST_{Mg/Ca}$, red) obtained on *Globigerinoides ruber* (p) (Hou et al., 2020b), alkenone-based SST ($SST_{Uk'37}$, black, this study), and TEX_{86}-based temperatures (T_{TEX86}, blue, this study), here using the surface calibration (Kim et al., 2010). Red, black, and blue triangles denote core-top values from multicore M125-55-8 for $SST_{Mg/Ca}$ (Hou et al., 2020b), $SST_{Uk'37}$ and T_{TEX86}, respectively. Shadings illustrate the respective calibration errors, lines represent 3-pt running means. (b) Difference between $SST_{Mg/Ca}$ and $SST_{Uk'37}$ and (c) $SST_{Uk'37}$ and T_{TEX86}, with blue shading indicating values exceeding the propagated error. (d) Benthic foraminifera $\delta^{18}O$ obtained on *Uvigerina* sp. of the same core for reference (Hou et al., 2020b). Thick lines in panels (a) to (c) represent three-point running averages. Marine Isotope Stages (MIS) are indicated by gray bars.

a threshold value for reliable T_{TEX86_H} estimates (Hopmans et al., 2004). A distinct maximum in BIT values is reached during late MIS 6 between 162–128 ka, with peak values of up to 0.88. This presumably high input of terrestrial organic material is also echoed by a parallel high in *n*-alkane concentrations (Figure 4), although *n*-alkane concentrations start to decline earlier during MIS 6 (at 139 ka) than BIT values. Despite the on average high BIT values, a good visual match between T_{TEX86_H} and BIT fluctuations appears only during 162–128 ka. However, there is no statistically significant correlation between these two parameters during this interval nor during the entire data set (entire interval: $r^2 = 0.03$; interval 162–128 ka: $r^2 = 0.05$) pointing at other factors than input of terrigenous GDGTs influencing T_{TEX86_H} variability (cf. discussion in Section 6.2) at our study site.

5.3. Upwelling and Productivity Indicators

The abundances of the oligotrophic, warm-water indicator *G. ruber* (p) and the upwelling-affiliated species *G. bulloides* in Core M125-55-7 are roughly anticorrelated (Figure 5b). *G. ruber* (p) shows the highest abundances during MIS 6 (around 19%, with a distinct drop to ~6% at ~140 ka) and after 90 ka, where peak values of 35% during MIS 5b are followed by values fluctuating around 19%. The abundance of *G. bulloides*, on the other hand, shows a broad plateau with peak values of 42% during MIS 5e-b (127–90 ka), with abrupt drops in abundance to values <5% before and after this interval. This pattern mimics *G. bulloides* abundances obtained on near-by core GL-74 during MIS 5c-a (Portilho-Ramos et al., 2015) (Figure 5b). Accumulation rates (AR) (Figure 6a)

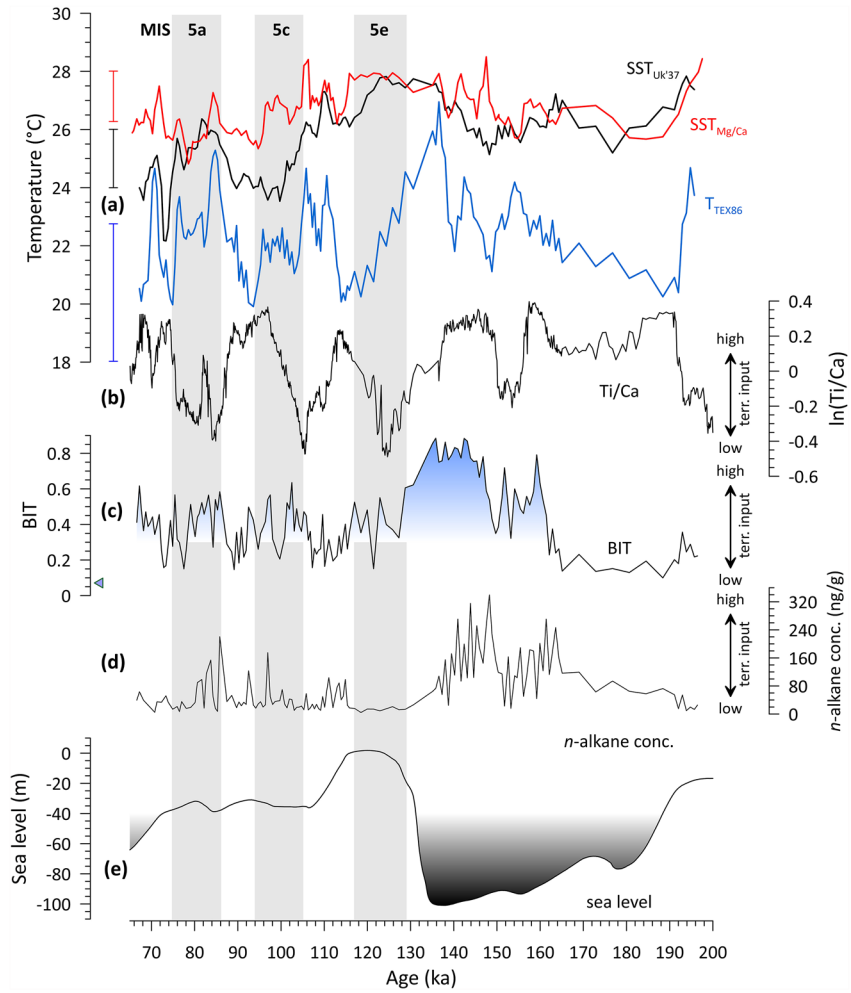

Figure 4. Proxies for terrigenous input obtained on piston core M125-55-7 compared to different temperature estimates from the same core for Marine Isotope Stages (MIS) 6–5. (a) Three-point running averages of Mg/Ca-based sea-surface temperature ($SST_{Mg/Ca,}$ red) obtained on *Globigerinoides ruber* (p) (Hou et al., 2020b), alkenone-based SST ($SST_{Uk'37}$, black, this study), and TEX_{86_H}-based temperatures (T_{TEX86}, blue, this study), here using the surface calibration (Kim et al., 2010); red, black and blue error bars correspond to the errors of $SST_{Mg/Ca}$, $SST_{Uk'37}$, and T_{TEX86_H} estimates, respectively. (b) Terrigenous siliciclastic input shown by the ln(Ti/Ca) record (Hou et al., 2020a). Terrigenous organic matter input represented by (c) the branched and isoprenoid tetraether index (blue triangle denotes core top value from multicore M125-55-8) and (d) *n*-alkane concentrations. (e) Global eustatic sea level (De Boer et al., 2014). The black shading indicates the 40 m isobath, which represents a threshold for flooding of the wide Abrolhos Bank shelf (cf. also Figure 1). Marine Isotope Stages (MIS) are indicated by gray bars.

essentially show the same picture as the species percentages, emphasizing the peak in *G. bulloides* productivity during MIS 5e and 5c as well as its absence during MIS 5a. Notably, during MIS 5a the planktic foraminiferal assemblages are dominated by warm-water affiliated *G. ruber* (w), in line with evidence for reduced upwelling intensity indicated by the low *G. bulloides* percentages.

Alkenone concentrations (Figure 5c), reflecting blooms of coccolithophorides, are fluctuating on a high level during MIS 6 until ~149 ka (at maximum 590 ng/g), when they drop to values below 10 ng/g until the end of MIS 5e. A second maximum in alkenone concentrations with up to 592 ng/g occurs during MIS 5d-b, with MIS 5a being characterized by moderate concentrations around 76 ng/g. Alkenone AR mimic this pattern, albeit the peak during MIS 6 is subdued compared to MIS 5d-b (Figure 6b).

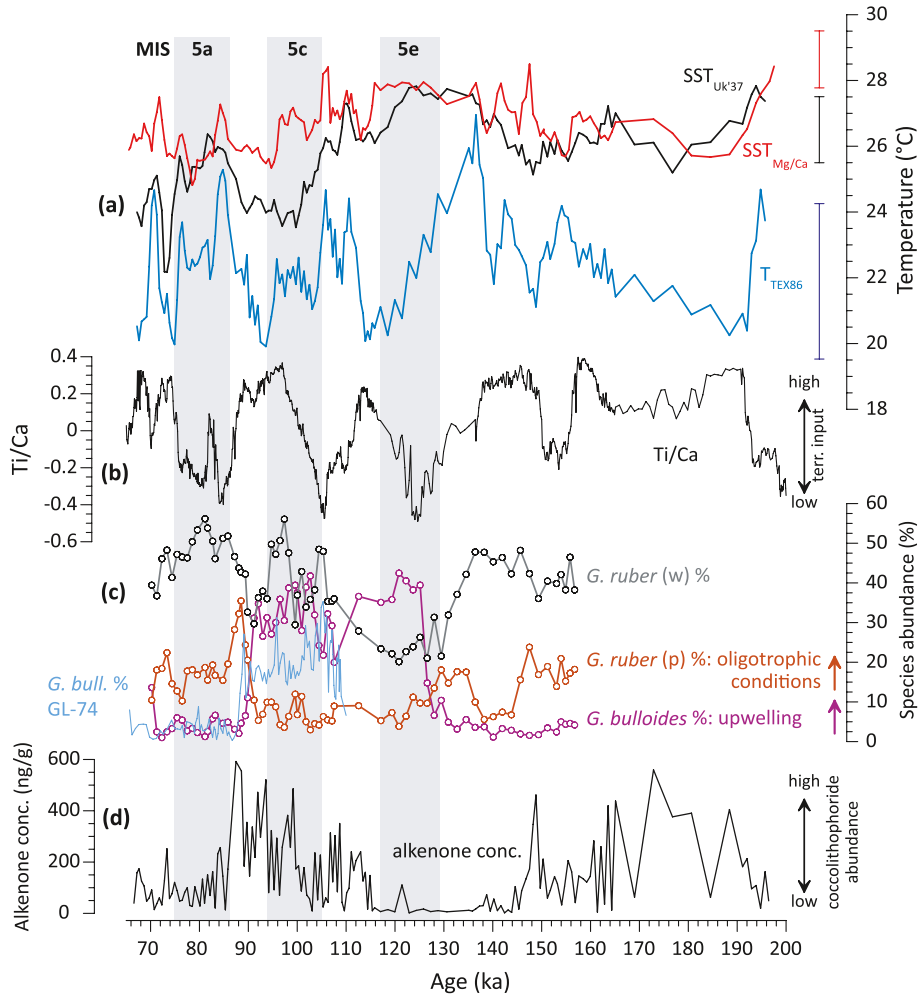

Figure 5. Proxies for marine productivity obtained on piston core M125-55-7 compared to different temperature estimates from the same core and a marine productivity proxy from a near-by core for Marine Isotope Stages (MIS) 6–5. (a) Three-point running averages of Mg/Ca-based sea-surface temperature ($SST_{Mg/Ca,}$ red) obtained on *Globigerinoides ruber* (p) (Hou et al., 2020b), alkenone-based SST ($SST_{Uk'37}$, black, this study), and TEX_{86_H}-based temperatures (T_{TEX86}, blue, this study), here using the surface calibration (Kim et al., 2010); red, black and blue error bars correspond to the errors of $SST_{Mg/Ca}$, $SST_{Uk'37}$, and T_{TEX86_H} estimates, respectively. (b) Terrigenous siliciclastic input shown by the ln(Ti/Ca) record (Hou et al., 2020a). (c) Marine productivity variations are reflected by the abundance (in % relative to total planktic foraminifera) of upwelling-affiliated *Globigerina bulloides* (thick purple line) versus oligotrophic, warm-water affiliated *G. ruber* (p) (red) and *G. ruber* (w) (dark green). In addition, *G. bulloides* percentages from near-by core GL-74 (Portilho-Ramos et al., 2015) (cf. Figure 1 for location) are depicted (thin blue line). (d) Alkenone concentrations as a proxy for the abundance of coccolithophorides in the water column. MIS are indicated by gray bars.

6. Discussion

In the following discussion we aim to assess (a) the robustness of each temperature proxy with regard to the a priori assumption that they are indicators of mean annual SST, (b) investigate the potential environmental factors influencing each temperature proxy signal, and (c) elaborate on the paleoceanographic implications of our findings.

6.1. Alkenone Versus Mg/Ca-Based SST Estimates

One of the major motivations of this study was to investigate whether the unexpected SST warming at the end of MIS 6 leading to an early plateauing of SST before the onset of MIS 5e (Hou et al., 2020b) is a feature that is particular to Mg/Ca-derived SST. We find that this SST signal is likewise present in the $SST_{Uk'37}$ record with

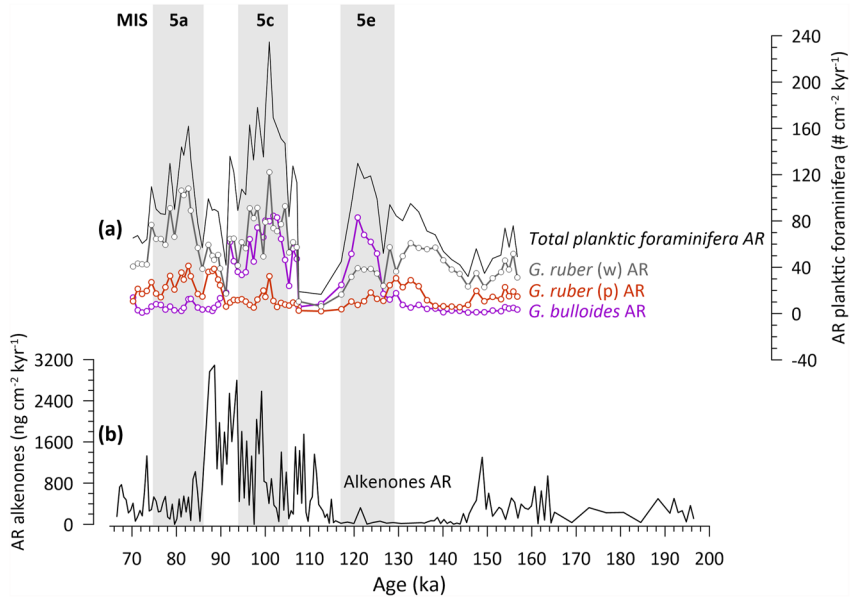

Figure 6. Accumulation rates of (a) planktic foraminifera (purple: *Globigerina bulloides*; red: *Globigerinoides ruber* (p); dark green: *G. ruber* (w); black: total planktic foraminifera) and (b) alkenones in piston core M125-55-7. Marine Isotope Stages are indicated by gray bars.

virtually identical temperatures during the interval 140–125 ka (Figures 3a and 3b). Thus, the enhanced SST warming at the end of MIS 6 appears to be a robust paleoceanographic signal and supports the accumulation of warm surface-water masses in the WTSA, likely as a result of strengthened southeast trade winds pushing warm waters toward South America (Hou et al., 2020b).

Although one could argue that both proxies may be biased toward the warm season, we infer that this scenario is an unlikely explanation for the warm SST during late MIS 6. As detailed in Leduc et al. (2010) and Bova

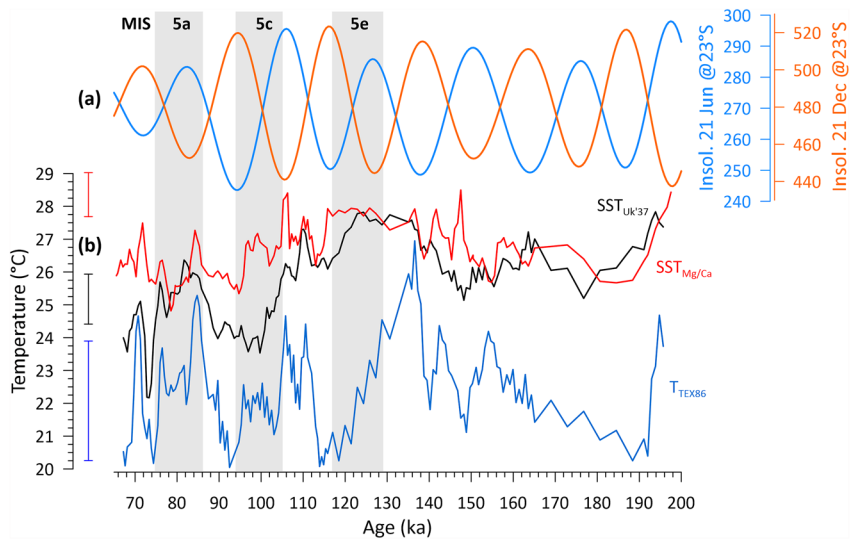

Figure 7. Insolation forcing relative to the respective temperature estimates. (a) Austral summer (orange) and winter (blue) insolation at 23°S (Laskar et al., 2004) compared to (b) three-point running averages of Mg/Ca-based sea-surface temperatures ($SST_{Mg/Ca,}$ red) obtained on *Globigerinoides ruber* (p) (Hou et al., 2020b), alkenone-based SST ($SST_{Uk'37}$, black, this study), and TEX_{86_H}-based temperatures (T_{TEX86}, blue, this study), here using the surface calibration (Kim et al., 2010); red, black, and blue error bars correspond to the errors of $SST_{Mg/Ca}$, $SST_{Uk'37}$, and T_{TEX86_H} estimates, respectively. Marine Isotope Stages are indicated by gray bars.

et al. (2021) a seasonal bias, particularly at low-latitude sites, should be evident when proxies follow the respective seasonal insolation curve, especially during interglacials, when other climate forcings (such as ice volume changes) are of minor importance. In the case of the SST data from M125-55-7, no synchronous insolation forcing on $SST_{Mg/Ca}$ and $SST_{Uk'37}$ can be observed. $SST_{Mg/Ca}$ does not show any correlation to neither austral summer or winter insolation (Figure 7) and thus appears to reflect annual mean SST. The choice of different $SST_{Mg/Ca}$ calibrations for *G. ruber* (pink) utilizing core top or sediment trap material from the tropical Atlantic (Anand et al., 2003; Regenberg et al., 2009) leads to higher temperature estimates which may be indicative of a summer bias of $SST_{Mg/Ca}$ (see Figure S1 in Supporting Information S1). However, since these equations are derived from non-reductively cleaned specimens, a methodological bias may be introduced in the temperature estimated even when correction for Mg-loss due to the reductive cleaning step is applied (Martin and Lea, 2002). Crucially, the long-term pattern of $SST_{Mg/Ca}$ changes remains the same regardless of calibration choice (Rosenthal et al., 2022).

On the other hand, $SST_{Uk'37}$ seems to follow summer insolation during parts of MIS 6 (but only until ∼160 ka) and winter insolation starting at MIS 5e (∼130 ka). However, both $SST_{Uk'37}$ and $SST_{Mg/Ca}$ are mostly overlapping within error (Figures 3a and 3b), hence, any potential seasonal bias in $SST_{Uk'37}$ is rather small, which is in line with the small modern seasonal SST difference of 2.7°C at the study site (Locarnini et al., 2018). For the interval MIS 5e-a, where $SST_{Uk'37}$ cooling relative to $SST_{Mg/Ca}$ occurs during winter insolation maxima (Figure 7), it might be assumed that coccolithophorides are predominantly thriving during the winter season, contrary to *G. ruber* (p) which represents annual mean conditions. This would also explain the deviation of $SST_{Uk'37}$ toward lower temperatures relative to $SST_{Mg/Ca}$ from MIS 5d onwards, with the caveat that this deviation is only for short intervals larger than the uncertainties of the SST estimates (e.g., MIS 5c; Figure 3b). Since high coccolithophoride abundances characterize phases of high productivity, a winter bias of $SST_{Uk'37}$ might be supported by the present-day observation that the chlorophyll maximum (and thus, primary productivity) on the Abrolhos Bank occurs during winter (Ghisolfi et al., 2015). This potential winter bias is also evident from studies on phytoplankton structures on the shelf and slope on the southeastern Brazilian Margin, south of 21°S (Rodrigues and McPhaden, 2014).

Interestingly, the insolation pacing of $SST_{Uk'37}$ during MIS 5 was particularly prominent during MIS 5c-a, but less so during MIS 5e. This appears odd, considering the high insolation amplitude during MIS 5e and the fact that sea level was high enough to submerge the Abrolhos Bank throughout the entire MIS 5 period (Figure 4e; De Boer et al., 2014). In this case, non-linear behavior between insolation and SST variations (Bova et al., 2022) might explain the lack of insolation pacing of $SST_{Uk'37}$ during MIS 5e. However, an additional factor might be that the dispersal of shelf-derived organic material to the slope may have been enhanced during intermediate sea level states (MIS 5c-a) (Figure 4e), as also supported by the high alkenone AR during MIS 5d-b (Figure 6b). Here, stronger hydrodynamic conditions (e.g., caused by wave activity and/or wind-induced currents) on the shallowly inundated shelf may have facilitated re-suspension of organic-rich material. Assuming that, like present, primary productivity on the Abrolhos Bank is highest during winter (Ghisolfi et al., 2015), the shelf-derived material might lead to a winter-bias of $SST_{Uk'37}$. Considering a sea-level influence, the ∼40 m isobath might act as a threshold, as when sea level is above 40 m wide areas of the Abrolhos Bank get inundated (Figure 1), a situation constantly achieved during MIS 5, but not during most of MIS 6 (Figure 4).

Notably, variations in upwelling related to the activity of the Vitória Eddy is unlikely to have impacted $SST_{Mg/Ca}$ and $SST_{Uk'37}$, as upwelling intensity (reflected by *G. bulloides* abundances and AR; Figures 5 and 6) does not fluctuate synchronously with $SST_{Mg/Ca}$ and $SST_{Uk'37}$ variations. Hence, its impact on the seasonality or habitat of the respective proxy carriers seems to have been rather negligible. Considering that the partial $SST_{Uk'37}$ alignment with winter insolation might also be a consequence of run-off variations by the Rio Doce (cf. the following Section 6.2), it appears that a direct impact of insolation on $SST_{Uk'37}$ is nearly impossible to constrain and is superposed by other factors such as fluctuations in the hydrological cycle or glacio-eustatic sea level.

6.2. TEX_{86}-Derived Temperatures—Influence by Terrigenous Input

Striking aspects of the T_{TEX86_H} record are its distinct deviation from the other two SST records in absolute values (even considering the high-temperature calibration) and its distinct millennial-scale variability during MIS 5 (Figure 3). Considering that $SST_{Uk'37}$ and $SST_{Mg/Ca}$ follow similar trends (despite the above discussed discrepancies), it is clear that T_{TEX86_H} does not reflect annual mean SST, even if core-top values suggest otherwise (Table 1). A seasonal bias is also unlikely because the T_{TEX86_H} amplitude of ∼10°C (Figure 3) far exceeds seasonal SST variations in the WTSA (Figure 1; Locarnini et al., 2018). Hence, other factors must have

influenced the T_{TEX86_H} signal. As we discuss in the following, these factors might include (a) contributions of terrestrial GDGTs and (b) variations in terrestrial input leading to a vertical migration of the oceanic TEX_{86} producers.

For most parts of the record, BIT values are >0.3, suggesting that a contamination of the T_{TEX86_H} signal by terrestrial GDGTs is likely. If terrigenous GDGTs were a major factor influencing the T_{TEX86_H} fluctuations, both parameters should show similar variations. This is indeed the case during the interval 162–128 ka, where maximum BIT values and high *n*-alkane concentrations both indicate strong input of terrestrial organic material (Figure 4). However, none of the peculiar fluctuations in T_{TEX86_H} in MIS 5 are mirrored by the BIT index. In fact, T_{TEX86_H} closely follows Ti/Ca ratios from the same core (Hou et al., 2020b). The Ti/Ca ratio reflects variations in Doce River run-off, with high (low) values characterizing high (low) terrigenous material input, in line with low (high) T_{TEX86_H}. On first sight, the significant match between T_{TEX86_H} and Ti/Ca ($r = -0.32$, $p < 0.05$) appears in line with the assumption of a direct influence of terrigenous input on the sedimentary GDGT composition. However, the lack of correlation between BIT and Ti/Ca ($r = 0.15$, $p = 0.41$) as well as BIT and T_{TEX86_H} ($r = 0.17$, $p = 0.17$) indicates that the terrigenous input of GDGTs was not the sole factor for the T_{TEX86_H} fluctuations during the studied time interval.

Based on the varying relationships between BIT, Ti/Ca, and T_{TEX86_H}, we infer that the record can be split into two phases characterized by different T_{TEX86_H} drivers: an interval from 162 to 128 ka during which T_{TEX86_H} is directly impacted by terrigenous GDGTs and the remainder of the record during which T_{TEX86_H} is indirectly impacted by terrigenous material leading to vertical migrations of the TEX_{86} producers. Regarding the intervals where Ti/Ca and T_{TEX86_H} match very well (200–162 and 128–68 ka), we infer that the enhanced input of suspension-load enhanced aggregate formation and the efficiency of downward transport of particulate organic material from the sea surface toward the pycnocline. Here, this material is consumed by the heterotrophic archaea producing the TEX_{86} constituents. Such a vertical migration of Thaumarchaeota as a response to enhanced downward transport of organic particulate material has also been inferred by Ceccopieri et al. (2018) from core top data from the southern Brazilian Margin. Likewise, a shift of Thaumarchaeota toward thermocline depth has been reconstructed from other regions such as the tropical Atlantic (Lopes dos Santos et al., 2010) and the equatorial Pacific and Caribbean (Hertzberg et al., 2016; Huguet et al., 2022; Seki et al., 2012) and was attributed to changes in the depth of the nitrate maximum (Könneke et al., 2005; Wuchter et al., 2006) as a response to changes in surface primary productivity. However, with respect to our record it appears rather unlikely that surface productivity itself was affected by enhanced run-off because foraminiferal abundances do not parallel the Ti/Ca record (Figures 4 and 5).

Interestingly, $SST_{Uk'37}$ parallels T_{TEX86_H} as well as Ti/Ca during MIS 5 ($SST_{Uk'37}$ vs. Ti/Ca: $r = -0.56$; $p = 0.01$), which might indicate that coccolithophorides also have changed their preferred depth, albeit not as pronouncedly as Thaumarchaeota because of the comparatively subdued $SST_{Uk'37}$ amplitude. In addition, enhanced freshwater input and light limitation by suspension load might have exerted environmental stress on the coccolithophorides, which has been demonstrated to cause a low-temperature bias of $SST_{Uk'37}$ (Crivellari et al., 2019; Häggi et al., 2015). Notably, such run-off influence on the coccolithophorides would also be capable to explain the insolation pacing of the $SST_{Uk'37}$ since higher austral summer insolation intensifies monsoonal rainfall in the catchment of the Doce River, which enhances run-off (Hou et al., 2020a), that result in colder $SST_{Uk'37}$. Given the anti-phased relationship between austral summer and winter insolation, the latter scenario may mimic the winter bias of $SST_{Uk'37}$ discussed in Section 6.1. Based on the comparison of the proxy data with the insolation curves, it is impossible to distinguish between these two options. However, the statistically significant correlation between $SST_{Uk'37}$ and Ti/Ca for MIS 5 suggests that run-off could have played a role in influencing $SST_{Uk'37}$, in addition to a potential seasonal bias.

Strikingly, the interval between 162–128 ka, which behaves differently from the remainder of the record, falls into a period of minimum sea level during MIS 6. Low sea level would produce a wide, subaerially exposed and vegetated Abrolhos Bank (Figure 1), providing a much larger and more proximal source of soil-derived GDGTs compared to periods of high sea level and a flooded Abrolhos Bank (i.e., 200–162 and 128–68 ka) (Figure 4). The influence of sea level on the BIT index is clearly evident during Termination II, when the abrupt increase in sea level at ∼132 ka corresponds to a strong reduction of BIT values (Figure 4). In addition, clay mineral analyses of Core M125-55-7 indicate that precipitation in the densely vegetated low-land catchment area of the Doce River was enhanced during late MIS 6 (Arndt et al., 2022; Hou et al., 2020a) which would also facilitate soil erosion

and thus increase BIT values. Hence, a combination of sea level variations and run-off changes in the hinterland may have caused the fluctuations in T_{TEX86_H}.

Hence, while vertical migrations of either Thaumarchaeota or coccolithophorides has been described from various oceanographic settings, the ultimate driver (e.g., nutrient availability, effectivity of vertical particle transport) needs to be carefully considered for each individual record.

7. Conclusions

In this study, we compare three established SST proxies (Mg/Ca on planktonic foraminifera, $U^{K'}_{37}$, and TEX_{86_H}) across MIS 6 to 5 analyzed on a sediment core from the Brazilian Margin. Although core top values of all three proxies agree well with annual mean SST, TEX_{86_H}-based temperatures diverge to distinctly lower temperatures than estimated via the other two proxies during most of the investigated interval. We argue that during MIS 6 a low sea level fostered the input of reworked terrestrial GDGTs (as indicated by a high BIT index) which biased the TEX_{86}-based temperatures. During MIS 5, we postulate a more indirect influence by increased sedimentary suspension load on TEX_{86_H}-temperatures via facilitated aggregate formation. This resulted in a more efficient vertical organic-matter transport through the water column causing the heterotrophic marine TEX_{86}-producers (Thaumarchaeota) to migrate beneath the mixed layer. While Mg/Ca and $U^{K'}_{37}$-based SST estimates are within errors similar during most of the record, an up to 2°C divergence of $U^{K'}_{37}$ SST toward colder values can be observed during MIS 5, where a pacing by austral winter insolation points at a seasonal bias potentially caused by enhanced winter-time blooms of coccolithophorides. In addition, our records provide evidence that $U^{K'}_{37}$ SST was likewise influenced by run-off variability either by vertical migration of the coccolithophorides into greater water depths and/or the influence of environmental stress on the proxy signal.

Albeit this caveat, both, Mg/Ca and $U^{K'}_{37}$-based SST, appear to be robust tracers of SST during glacial as well as interglacial boundary conditions in the WTSA, while the use of TEX_{86} should be done with caution. The new data also corroborates previous evidence for an anomalous SST warming occurring over the course of the MIS 6 glacial.

Data Availability Statement

All data published in this paper are available on the PANGAEA database (Bahr et al., 2023).

Acknowledgments
We acknowledge support by Captain Hammacher and the crew of R/V METEOR during the M125 Expedition. AB was supported by DFG Grant BA3809/9, AJ acknowledges financial support from DFG (Grant 268236062-SFB 1211). ALA is a CNPq senior researcher (Grant 302521/2017-8). CMC acknowledges financial support from FAPESP (Grants 2018/15123-4 and 2019/24349-9) CNPq (Grant 312458/2020-7) and the Alexander von Humboldt Foundation. OF acknowledges funding by DFG Grant FR 2544/14. We are indebted to Stefanie Kaboth-Bahr for running the BAYSPAR code in Matlab. Open Access funding enabled and organized by Projekt DEAL.

References

Anand, P., Elderfield, H., & Conte, M. H. (2003). Calibration of Mg/Ca thermometry in planktonic foraminifera from a sediment trap series. *Paleoceanography*, *18*(2), 1050.

Antoine, D., André, J. M., & Morel, A. (1996). Oceanic primary production: 2. Estimation at global scale from satellite (coastal zone color scanner) chlorophyll. *Global Biogeochemical Cycles*, *10*(1), 57–69. https://doi.org/10.1029/95gb02832

Arndt, I., Voigt, S., Petschick, R., Hou, A., Raddatz, J., Albuquerque, A. L. S., & Bahr, A. (2022). Spatiotemporal discharge variability of the Doce River in SE Brazil during MIS 6 and 5. *Frontiers in Earth Science*, *10*, 864381. https://doi.org/10.3389/feart.2022.864381

Arruda, W. Z., Campos, E. J., Zharkov, V., Soutelino, R. G., & da Silveira, I. C. (2013). Events of equatorward translation of the Vitoria Eddy. *Continental Shelf Research*, *70*, 61–73. https://doi.org/10.1016/j.csr.2013.05.004

Arruda, W. Z., & da Silveira, I. C. (2019). Dipole-induced central water extrusions south of Abrolhos Bank (Brazil, 20.5 oS). *Continental Shelf Research*, *188*, 103976. https://doi.org/10.1016/j.csr.2019.103976

Ausín, B., Haghipour, N., Bruni, E., & Eglinton, T. (2022). The influence of lateral transport on sedimentary alkenone paleoproxy signals. *Biogeosciences*, *19*(3), 613–627. https://doi.org/10.5194/bg-19-613-2022

Bahr, A., Jaeschke, A., Hou, A. M. X., Meier, K. J. F., Chiessi, C. M., Albuquerque, A. L., & Friedrich, O. (2023). Alkenone and TEX86 data for MIS 6 to 5 on the Brazilian margin [Dataset]. PANGAEA. https://doi.org/10.1594/PANGAEA.956207

Bahr, A., Spadano Albuquerque, A., Ardenghi, N., Batenburg, S., Bayer, M., Catunda, M., et al. (2016). *South American hydrological balance and paleoceanography during the Late Pleistocene and Holocene (SAMBA)–Cruise No. M125, March 21–April 15, 2016-Rio de Janeiro (Brazil)–Fortaleza (Brazil)*. DFG-Senatskommission für Ozeanographie.

Bard, E. (2001). Comparison of alkenone estimates with other paleotemperature proxies. *Geochemistry, Geophysics, Geosystems*, *2*(1), 1002. https://doi.org/10.1029/2000gc000050

Benthien, A., & Müller, P. J. (2000). Anomalously low alkenone temperatures caused by lateral particle and sediment transport in the Malvinas Current region, western Argentine Basin. *Deep Sea Research Part I: Oceanographic Research Papers*, *47*(12), 2369–2393. https://doi.org/10.1016/s0967-0637(00)00030-3

Blanz, T., Emeis, K.-C., & Siegel, H. (2005). Controls on alkenone unsaturation ratios along the salinity gradient between the open ocean and the Baltic Sea. *Geochimica et Cosmochimica Acta*, *69*(14), 3589–3600. https://doi.org/10.1016/j.gca.2005.02.026

Bova, S., Rosenthal, Y., Liu, Z., Godad, S. P., & Yan, M. (2021). Seasonal origin of the thermal maxima at the Holocene and the last interglacial. *Nature*, *589*(7843), 548–553. https://doi.org/10.1038/s41586-020-03155-x

Bova, S., Rosenthal, Y., Liu, Z., Yan, M., Broccoli, A. J., Godad, S. P., et al. (2022). Reply to: Concerns of assuming linearity in the reconstruction of thermal maxima. *Nature*, *607*(7920), E15–E18. https://doi.org/10.1038/s41586-022-04832-9

Brassell, S. C., Eglinton, G., Marlowe, I., Pflaumann, U., & Sarnthein, M. (1986). Molecular stratigraphy: A new tool for climatic assessment. *Nature*, *320*(6058), 129–133. https://doi.org/10.1038/320129a0

Castro, B. M., Brandini, F. P., Pires-Vanin, A. M. S., & Miranda, L. B. (2006). Multidisciplinary oceanographic processes on the Western Atlantic continental shelf between 4 N and 34 S. *Sea*, *11*, 209–251.

Ceccopieri, M., Carreira, R. S., Wagener, A. L., Hefter, J. H., & Mollenhauer, G. (2018). On the application of alkenone-and GDGT-based temperature proxies in the south-eastern Brazilian continental margin. *Organic Geochemistry*, *126*, 43–56. https://doi.org/10.1016/j.orggeochem.2018.10.009

Cléroux, C., Lynch-Stieglitz, J., Schmidt, M. W., Cortijo, E., & Duplessy, J.-C. (2009). Evidence for calcification depth change of *Globorotalia truncatulinoides* between deglaciation and Holocene in the western Atlantic Ocean. *Marine Micropaleontology*, *73*(1–2), 57–61. https://doi.org/10.1016/j.marmicro.2009.07.001

Crivellari, S., Chiessi, C. M., Kuhnert, H., Häggi, C., da Costa Portilho-Ramos, R., Zeng, J.-Y., et al. (2018). Increased Amazon freshwater discharge during late Heinrich Stadial 1. *Quaternary Science Reviews*, *181*, 144–155. https://doi.org/10.1016/j.quascirev.2017.12.005

Crivellari, S., Chiessi, C. M., Kuhnert, H., Häggi, C., Mollenhauer, G., Hefter, J., et al. (2019). Thermal response of the western tropical Atlantic to slowdown of the Atlantic meridional Overturning circulation. *Earth and Planetary Science Letters*, *519*, 120–129. https://doi.org/10.1016/j.epsl.2019.05.006

De Boer, B., Lourens, L. J., & Van De Wal, R. S. (2014). Persistent 400,000-year variability of Antarctic ice volume and the carbon cycle is revealed throughout the Plio-Pleistocene. *Nature Communications*, *5*(1), 2999. https://doi.org/10.1038/ncomms3999

Dekens, P. S., Lea, D. W., Pak, D. K., & Spero, H. J. (2002). Core top calibration of Mg/Ca in tropical foraminifera: Refining paleotemperature estimation. *Geochemistry, Geophysics, Geosystems*, *3*(4), 1–29. https://doi.org/10.1029/2001gc000200

Ebisuzaki, W. (1997). A method to estimate the statistical significance of a correlation when the data are serially correlated. *Journal of Climate*, *10*(9), 2147–2153. https://doi.org/10.1175/1520-0442(1997)010<2147:amtets>2.0.co;2

Ferguson, J. E., Henderson, G. M., Kucera, M., & Rickaby, R. E. M. (2008). Systematic change of foraminiferal Mg/Ca ratios across a strong salinity gradient. *Earth and Planetary Science Letters*, *265*(1–2), 153–166. https://doi.org/10.1016/j.epsl.2007.10.011

Gaeta, S. A., Lorenzzetti, J. A., Miranda, L. D., Susini-Ribeiro, S., Pompeu, M., & Araujo, C. (1999). The Vitória Eddy and its relation to the phytoplankton biomass and primary productivity during the austral fall of 1995. *Archive of Fishery and Marine Research*, *47*(2/3), 253–270.

Garzoli, S. L., Dong, S., Fine, R., Meinen, C. S., Perez, R. C., Schmid, C., et al. (2015). The fate of the deep western boundary current in the South Atlantic. *Deep Sea Research Part I: Oceanographic Research Papers*, *103*, 125–136. https://doi.org/10.1016/j.dsr.2015.05.008

Ghisolfi, R. D., Pereira da Silva, M., Thomaz dos Santos, F., Servino, R. N., Cirano, M., & Thompson, F. L. (2015). Physical forcing mechanisms controlling the variability of chlorophyll-*a* over the Royal-Charlotte and Abrolhos Banks—Eastern Brazilian shelf. *PLoS One*, *10*(2), e0117082. https://doi.org/10.1371/journal.pone.0117082

Govin, A., Holzwarth, U., Heslop, D., Ford Keeling, L., Zabel, M., Mulitza, S., et al. (2012). Distribution of major elements in Atlantic surface sediments (36°N–49°S): Imprint of terrigenous input and continental weathering. *Geochemistry, Geophysics, Geosystems*, *13*(1), Q01013. https://doi.org/10.1029/2011gc003785

Häggi, C., Chiessi, C. M., & Schefuß, E. (2015). Testing the D/H ratio of alkenones and palmitic acid as salinity proxies in the Amazon Plume. *Biogeosciences*, *12*(23), 7239–7249. https://doi.org/10.5194/bg-12-7239-2015

Hertzberg, J. E., Schmidt, M. W., Bianchi, T. S., Smith, R. W., Shields, M. R., & Marcantonio, F. (2016). Comparison of eastern tropical Pacific TEX86 and Globigerinoides ruber Mg/Ca derived sea surface temperatures: Insights from the Holocene and last glacial maximum. *Earth and Planetary Science Letters*, *434*, 320–332. https://doi.org/10.1016/j.epsl.2015.11.050

Hopmans, E. C., Schouten, S., & Sinninghe Damsté, J. S. (2016). The effect of improved chromatography on GDGT-based palaeoproxies. *Organic Geochemistry*, *93*, 1–6. https://doi.org/10.1016/j.orggeochem.2015.12.006

Hopmans, E. C., Weijers, J. W. H., Schefuß, E., Herfort, L., Sinninghe Damste, J. S., & Schouten, S. (2004). A novel proxy for terrestrialorganic matter in sediments based on branched and isoprenoid tetraether lipids. *Earth and Planetary Science Letters*, *224*(1–2), 107–116. https://doi.org/10.1016/j.epsl.2004.05.012

Hou, A., Bahr, A., Raddatz, J., Voigt, S., Greule, M., Albuquerque, A. L., et al. (2020a). Insolation and greenhouse gas forcing of the South American Monsoon System across three Glacial-Interglacial cycles. *Geophysical Research Letters*, *47*(14), e2020GL087948. https://doi.org/10.1029/2020gl087948

Hou, A., Bahr, A., Schmidt, S., Strebl, C., Albuquerque, A. L., Chiessi, C. M., & Friedrich, O. (2020b). Forcing of western tropical South Atlantic sea surface temperature across three glacial-interglacial cycles. *Global and Planetary Change*, *188*, 103150. https://doi.org/10.1016/j.gloplacha.2020.103150

Huguet, C., Jaeschke, A., & Rethemeyer, J. (2022). Paleoclimatic and palaeoceanographic changes coupled to the Panama Isthmus closing (13–4 Ma) using organic proxies. *Palaeogeography, Palaeoclimatology, Palaeoecology*, *601*, 111139. https://doi.org/10.1016/j.palaeo.2022.111139

Huguet, C., Kim, J.-H., de Lange, G. J., Sinninghe Damsté, J. S., & Schouten, S. (2009). Effects of long term oxic degradation on the U37K′, TEX86 and BIT organic proxies. *Organic Geochemistry*, *40*(12), 1188–1194. https://doi.org/10.1016/j.orggeochem.2009.09.003

Huguet, C., Kim, J.-H., Sinninghe Damsté, J. S., & Schouten, S. (2006). Reconstruction of sea surface temperature variations in the Arabian Sea over the last 23 kyr using organic proxies (TEX86 and U37K′).

Hurley, S. J., Lipp, J. S., Close, H. G., Hinrichs, K.-U., & Pearson, A. (2018). Distribution and export of isoprenoid tetraether lipids in suspended particulate matter from the water column of the Western Atlantic Ocean. *Organic Geochemistry*, *116*, 90–102. https://doi.org/10.1016/j.orggeochem.2017.11.010

Jentzen, A., Schönfeld, J., Weiner, A. K., Weinkauf, M. F., Nürnberg, D., & Kučera, M. (2019). Seasonal and interannual variability in population dynamics of planktic foraminifers off Puerto Rico (Caribbean Sea). *Journal of Micropalaeontology*, *38*(2), 231–247. https://doi.org/10.5194/jm-38-231-2019

Kim, J.-H., Romero, O. E., Lohmann, G., Donner, B., Laepple, T., Haam, E., & Sinninghe Damsté, J. S. (2012). Pronounced subsurface cooling of North Atlantic waters off northwest Africa during Dansgaard–Oeschger interstadials. *Earth and Planetary Science Letters*, *339*, 95–102. https://doi.org/10.1016/j.epsl.2012.05.018

Kim, J.-H., Van der Meer, J., Schouten, S., Helmke, P., Willmott, V., Sangiorgi, F., et al. (2010). New indices and calibrations derived from the distribution of crenarchaeal isoprenoid tetraether lipids: Implications for past sea surface temperature reconstructions. *Geochimica et Cosmochimica Acta*, *74*(16), 4639–4654. https://doi.org/10.1016/j.gca.2010.05.027

Könneke, M., Bernhard, A. E., de La Torre, J. R., Walker, C. B., Waterbury, J. B., & Stahl, D. A. (2005). Isolation of an autotrophic ammonia-oxidizing marine archaeon. *Nature*, *437*(7058), 543–546. https://doi.org/10.1038/nature03911

Kusch, S., Eglinton, T. I., Mix, A. C., & Mollenhauer, G. (2010). Timescales of lateral sediment transport in the Panama Basin as revealed by radiocarbon ages of alkenones, total organic carbon and foraminifera. *Earth and Planetary Science Letters*, *290*(3–4), 340–350. https://doi.org/10.1016/j.epsl.2009.12.030

Laskar, J., Robutel, P., Joutel, F., Gastineau, M., Correia, A., & Levrard, B. (2004). A long-term numerical solution for the insolation quantities of the Earth. *Astronomy & Astrophysics*, *428*(1), 261–285. https://doi.org/10.1051/0004-6361:20041335

Leduc, G., Schneider, R., Kim, J. H., & Lohmann, G. (2010). Holocene and Eemian sea surface temperature trends as revealed by alkenone and Mg/Ca paleothermometry. *Quaternary Science Reviews*, *29*(7–8), 989–1004. https://doi.org/10.1016/j.quascirev.2010.01.004

Lisiecki, L. E., & Raymo, M. E. (2005). A Pliocene-Pleistocene stack of 57 globally distributed benthic delta O-18 records. *Paleoceanography*, *20*(1), PA1003.

Locarnini, M., Mishonov, A., Baranova, O., Boyer, T., Zweng, M., Garcia, H., et al. (2018). World ocean atlas 2018, volume 1: Temperature.

Lopes dos Santos, R. A., Prange, M., Castañeda, I. S., Schefuß, E., Mulitza, S., Schulz, M., et al. (2010). Glacial–interglacial variability in Atlantic meridional overturning circulation and thermocline adjustments in the tropical North Atlantic. *Earth and Planetary Science Letters*, *300*(3), 407–414. https://doi.org/10.1016/j.epsl.2010.10.030

Martin, P. A., & Lea, D. W. (2002). A simple evaluation of cleaning procedures on fossil benthic foraminiferal Mg/Ca. *Geochemistry, Geophysics, Geosystems*, *3*(10), 8401–8408. https://doi.org/10.1029/2001gc000280

Mémery, L., Arhan, M., Alvarez-Salgado, X., Messias, M.-J., Mercier, H., Castro, C., & Rios, A. (2000). The water masses along the western boundary of the south and equatorial Atlantic. *Progress in Oceanography*, *47*(1), 69–98. https://doi.org/10.1016/s0079-6611(00)00032-x

Meyers, S. (2014). Astrochron: An R package for astrochronology. Retrieved from https://cran.r-project.org/web/packages/astrochron/index.html

Mollenhauer, G., Eglinton, T. I., Hopmans, E. C., & Sinninghe Damsté, J. S. (2008). A radiocarbon-based assessment of the preservation characteristics of crenarchaeol and alkenones from continental margin sediments. *Organic Geochemistry*, *39*(8), 1039–1045. https://doi.org/10.1016/j.orggeochem.2008.02.006

Müller, P. J., Kirst, G., Ruhland, G., von Storch, I., & Rosell-Melé, A. (1998). Calibration of the alkenone paleotemperature index Uk37' based on core-tops from the eastern South Atlantic and the global ocean (60°N-60°S). *Geochimica et Cosmochimica Acta*, *62*(10), 1757–1772. https://doi.org/10.1016/s0016-7037(98)00097-0

Novak, J., McGrath, S. M., Wang, K. J., Liao, S., Clemens, S. C., Kuhnt, W., & Huang, Y. (2022). U38MEK′ Expands the linear dynamic range of the alkenone sea surface temperature proxy. *Geochimica et Cosmochimica Acta*, *328*, 207–220. https://doi.org/10.1016/j.gca.2022.04.021

Oliveira, K. S. S., & Quaresma, V. D. S. (2017). Temporal variability in the suspended sediment load and streamflow of the Doce River. *Journal of South American Earth Sciences*, *78*, 101–115. https://doi.org/10.1016/j.jsames.2017.06.009

Peeters, F. J., Brummer, G.-J. A., & Ganssen, G. (2002). The effect of upwelling on the distribution and stable isotope composition of Globigerina bulloides and Globigerinoides ruber (planktic foraminifera) in modern surface waters of the NW Arabian Sea. *Global and Planetary Change*, *34*(3–4), 269–291. https://doi.org/10.1016/s0921-8181(02)00120-0

Pena, L. D., Calvo, E., Cacho, I., Eggins, S., & Pelejero, C. (2005). Identification and removal of Mn-Mg-rich contaminant phases on foraminiferal tests: Implications for Mg/Ca past temperature reconstructions. *Geochemistry, Geophysics, Geosystems*, *6*(9), Q09P02. https://doi.org/10.1029/2005gc000930

Peterson, R. G., & Stramma, L. (1991). Upper-level circulation in the South Atlantic Ocean. *Progress in Oceanography*, *26*(1), 1–73. https://doi.org/10.1016/0079-6611(91)90006-8

Portilho-Ramos, R., Ferreira, F., Calado, L., Frontalini, F., & de Toledo, M. B. (2015). Variability of the upwelling system in the southeastern Brazilian margin for the last 110,000 years. *Global and Planetary Change*, *135*, 179–189. https://doi.org/10.1016/j.gloplacha.2015.11.003

Prahl, F. G., & Wakeham, S. G. (1987). Calibration of unsaturation patterns in long-chain ketone compositions for palaeotemperature assessment. *Nature*, *330*(6146), 367–369. https://doi.org/10.1038/330367a0

Raddatz, J., Titschack, J., Frank, N., Freiwald, A., Conforti, A., Osborne, A., et al. (2020). Solenosmilia variabilis-bearing cold-water mounds off Brazil.

Regenberg, M., Nürnberg, D., Schönfeld, J., & Reichert, G.-J. (2007). Early diagenetic overprint in Caribbean sediment cores and its effect on the geochemical composition of planktonic foraminifera. *Biogeosciences*, *4*(6), 957–973. https://doi.org/10.5194/bg-4-957-2007

Regenberg, M., Steph, S., Nürnberg, D., Tiedemann, R., & Garbe-Schönberg, D. (2009). Calibrating Mg/Ca ratios of multiple planktonic foraminiferal species with $d^{18}O$-calcification temperatures: Paleothermometry for the upper water column. *Earth and Planetary Science Letters*, *278*(3–4), 324–336. https://doi.org/10.1016/j.epsl.2008.12.019

Rodrigues, R. R., & McPhaden, M. J. (2014). Why did the 2011–2012 La Niña cause a severe drought in the Brazilian Northeast? *Geophysical Research Letters*, *41*(3), 1012–1018. https://doi.org/10.1002/2013gl058703

Rodrigues, R. R., Rothstein, L. M., & Wimbush, M. (2007). Seasonal variability of the South equatorial current bifurcation in the Atlantic Ocean: A numerical study. *Journal of Physical Oceanography*, *37*(1), 16–30. https://doi.org/10.1175/jpo2983.1

Rosenthal, Y., Bova, S., & Zhou, X. (2022). A user guide for choosing planktic foraminiferal Mg/Ca-temperature calibrations. *Paleoceanography and Paleoclimatology*, *37*(6), e2022PA004413. https://doi.org/10.1029/2022pa004413

Salgueiro, E., Voelker, A., Abrantes, F., Meggers, H., Pflaumann, U., Lončarić, N., et al. (2008). Planktonic foraminifera from modern sediments reflect upwelling patterns off Iberia: Insights from a regional transfer function. *Marine Micropaleontology*, *66*(3–4), 135–164. https://doi.org/10.1016/j.marmicro.2007.09.003

Santos, T. P., Lessa, D. O., Venancio, I. M., Chiessi, C. M., Mulitza, S., Kuhnert, H., et al. (2017). Prolonged warming of the Brazil Current precedes deglaciations. *Earth and Planetary Science Letters*, *463*, 1–12. https://doi.org/10.1016/j.epsl.2017.01.014

Schlitzer, R. (2009). Ocean data View. Retrieved from http://odv.awi.de

Schmid, C., Schäfer, H., Zenk, W., & Podestá, G. (1995). The Vitória eddy and its relation to the Brazil Current. *Journal of Physical Oceanography*, *25*(11), 2532–2546. https://doi.org/10.1175/1520-0485(1995)025<2532:tveair>2.0.co;2

Schmuker, B., & Schiebel, R. (2002). Planktic foraminifers and hydrography of the eastern and northern Caribbean Sea. *Marine Micropaleontology*, *46*(3–4), 387–403. https://doi.org/10.1016/s0377-8398(02)00082-8

Schouten, S., Hopmans, E. C., Schefuß$_s$, E., & Sinninghe Damste, J. S. (2002). Distributional variations in marine crenarchaeotal membrane lipids: A new tool for reconstructing ancient sea water temperatures? *Earth and Planetary Science Letters*, *204*(1–2), 265–274. https://doi.org/10.1016/s0012-821x(02)00979-2

Schouten, S., Huguet, C., Hopmans, E. C., Kienhuis, M. V., & Sinninghe Damsté, J. S. (2007). Analytical methodology for TEX86 paleothermometry by high-performance liquid chromatography/atmospheric pressure chemical ionization-mass spectrometry. *Analytical Chemistry*, *79*(7), 2940–2944. https://doi.org/10.1021/ac062339v

Seki, O., Schmidt, D. N., Schouten, S., Hopmans, E. C., Sinninghe Damsté, J. S., & Pancost, R. D. (2012). Paleoceanographic changes in the eastern equatorial Pacific over the last 10 Myr. *Paleoceanography and Paleoclimatology*, *27*(3), 1–14. https://doi.org/10.1029/2011pa002158

Shrivastav, A., Singh, A. K., Sinha, D. K., Kaushik, T., Singh, V. P., & Mallick, K. (2016). Significance of Globigerina bulloides d'orbigny: A foraminiferal proxy for palaeomonsoon and past upwelling records. *Journal of Climate Change*, *2*(2), 99–110. https://doi.org/10.3233/jcc-160021

Stramma, L. (1989). The Brazil Current transport south of 23 S. *Deep-Sea Research, Part A: Oceanographic Research Papers*, *36*(4), 639–646. https://doi.org/10.1016/0198-0149(89)90012-5

Stramma, L., & England, M. (1999). On the water masses and mean circulation of the South Atlantic Ocean. *Journal of Geophysical Research*, *104*(C9), 20863–20883. https://doi.org/10.1029/1999jc900139

Tierney, J. E., & Tingley, M. P. (2014). A Bayesian, spatially-varying calibration model for the TEX86 proxy. *Geochimica et Cosmochimica Acta*, *127*, 83–106. https://doi.org/10.1016/j.gca.2013.11.026

Wuchter, C., Schouten, S., Wakeham, S. G., & Sinninghe Damsté, J. S. (2006). Archaeal tetraether membrane lipid fluxes in the northeastern Pacific and the Arabian Sea: Implications for TEX86 paleothermometry. *Paleoceanography*, *21*(4), 1944. https://doi.org/10.1029/2006pa001279

Zhang, Y. G., & Liu, X. (2018). Export depth of the TEX86 signal. *Paleoceanography and Paleoclimatology*, *33*(7), 666–671. https://doi.org/10.1029/2018pa003337

Zweng, M., Seidov, D., Boyer, T., Locarnini, M., Garcia, H., Mishonov, A., et al. (2019). World ocean atlas 2018, volume 2: Salinity.